THE JOURNAL OF BIOLOGICAL CHEMISTRY VOL. 284, NO. 29, pp. 19533–19543, July 17, 2009

Pirenzepine Promotes the Dimerization of Muscarinic M1 Receptors through a Three-step Binding Process*[S]

Received for publication, February 4, 2009, and in revised form, May 5, 2009 Published, JBC Papers in Press, May 18, 2009, DOI 10.1074/jbc.M109.017145

Brigitte Ilien[‡1], Nicole Glasser[§], Jean-Pierre Clamme[§], Pascal Didier[§], Etienne Piemont[§], Raja Chinnappan[§], Sandrine B. Daval[‡2], Jean-Luc Galzi[‡], and Yves Mely[§]

From the [‡]Département Biotechnologies des Interactions Moléculaires, Institut de Recherche de l'Ecole de Biotechnologie de Strasbourg, FRE 3211, Université de Strasbourg, 67412 Illkirch and the [§]Laboratoire de Biophotonique et Pharmacologie, UMR 7213 CNRS, Faculté de Pharmacie, Université de Strasbourg, 67401 Illkirch, France

Ligand binding to G protein-coupled receptors is a complex process that involves sequential receptor conformational changes, ligand translocation, and possibly ligand-induced receptor oligomerization. Binding events at muscarinic acetylcholine receptors are usually interpreted from radioligand binding studies in terms of two-step ligand-induced receptor isomerization. We report here, using a combination of fluorescence approaches, on the molecular mechanisms for Bodipy-pirenzepine binding to enhanced green fluorescent protein (EGFP)-fused muscarinic M1 receptors in living cells. Real time monitoring, under steady-state conditions, of the strong fluorescence energy transfer signal elicited by this interaction permitted a fine kinetic description of the binding process. Time-resolved fluorescence measurements allowed us to identify discrete EGFP lifetime species and to follow their redistribution upon ligand binding. Fluorescence correlation spectroscopy, with EGFP brightness analysis, showed that EGFP-fused muscarinic M1 receptors predominate as monomers in the absence of ligand and dimerize upon pirenzepine binding. Finally, all these experimental data could be quantitatively reconciled into a three-step mechanism, with four identified receptor conformational states. Fast ligand binding to a peripheral receptor site initiates a sequence of conformational changes that allows the ligand to access to inner regions of the protein and drives ligand-receptor complexes toward a high affinity dimeric state.

G protein-coupled receptors (GPCRs)[3] trigger a wide palette of signaling pathways (1, 2), including G protein-independent responses (3). These receptors display multiple conformational and functional states, dependent on the cellular context, differentially selected and stabilized by ligands, and discriminated by downstream protein partners (4–9). The occurrence of distinct receptor conformational species is supported by structural arguments provided by metal ion site engineering (10) or *in situ* disulfide cross-linking (11) and by direct monitoring of receptor intramolecular rearrangements through fluorescence-based methods (for reviews see Refs. 8, 9, 12).

Few studies focused on the initial ligand binding step, its kinetic description, and its relationship with functionally relevant receptor conformational states. These aspects were addressed by monitoring intermolecular fluorescence resonance energy transfer (FRET) between a GFP-tagged receptor (donor) and a fluorescent ligand (acceptor). Both neurokinin A binding to class A tachykinin NK2 receptors (4, 13) and parathyroid hormone binding to class B parathyroid hormone receptors (14) proceeded in two steps, featuring two kinetically distinguishable conformational states. Whether such biphasic binding reactions are a general feature of GPCRs, independent on the pharmacological nature of the ligand, and whether they reflect different receptor functional states or sequential binding steps remain important questions to be elucidated.

Muscarinic cholinergic receptors (15) display complex antagonist binding mechanisms, classically interpreted according to a two-step isomerization model (16–20). More recently, a combination of point mutations and irreversible affinity labeling of the M1 receptor led to the proposal of a tandem two-site model (21), with ligand translocation from a peripheral site toward a more central receptor binding domain and the possibility for the receptor to bind two ligand molecules. All these data, however, are from radioligand binding studies, performed on membrane preparations and under conditions poorly compatible with fine temporal resolution of binding events and characterization of intermediate conformational species.

We previously reported that human muscarinic M1 receptor constructs (fused to EGFP at their N terminus) and several fluorescent derivatives of the antagonist pirenzepine behave as ideal donor-acceptor pairs for a robust and sensitive FRET-based binding assay (22, 23). These studies already pointed to the biphasic character of the association of these ligands to M1 receptors and prompted us to examine in more detail the interaction of Bodipy-pirenzepine (BoPz) with the already described EGFP(Δ17)hM1receptor chimera, stably expressed at the surface of living HEK cells.

* This work was supported in part by CNRS, INSERM, and the Université de Strasbourg.

[S] The on-line version of this article (available at http://www.jbc.org) contains a supplemental table and equations.

[1] To whom correspondence should be addressed: Institut de Recherche de l'Ecole de Biotechnologie de Strasbourg, Bvd. S. Brant-BP 10413, 67412 Illkirch Cedex, France. Tel.: 33-390-24-47-38; Fax: 33-390-24-48-29; E-mail: ilien@esbs.u-strasbg.fr.

[2] Recipient of a grant from the Association Nationale de la Recherche Technique, Convention CIFRE 564/2005.

[3] The abbreviations used are: GPCR, G protein-coupled receptor; GFP, green fluorescent protein; EGFP, enhanced green fluorescent protein; GPI, glycosylphosphatidylinositol; DMSO, dimethyl sulfoxide; FRET, fluorescence resonance energy transfer; TCSPC, time-correlated single photon counting; FCS, fluorescence correlation spectroscopy; QNB, [^{3}H]quinuclidinyl [*phenyl*-4-^{3}H]benzilate; NMS, [*N-methyl*-^{3}H]scopolamine; BoPz, Bodipy-pirenzepine; BSA, bovine serum albumin; HEK, human embryonic kidney; TMR, tetramethylrhodamine; Pz, pirenzepine.

In this study, real time monitoring of EGFP emission intensity as a function of BoPz concentration was performed to obtain a fine kinetic description of the binding process. Analysis of the distribution pattern of EGFP-excited lifetime species by time-correlated single photon counting (TCSPC) on cell suspensions was undertaken to detect discrete receptor conformational states and to check for their possible redistribution upon BoPz binding. Ligand-induced receptor dimerization was examined by fluorescence correlation spectroscopy using the same EGFP(Δ17)hM1-expressing cells. Finally, a unique three-step mechanism whereby BoPz promotes receptor dimerization was found to reconcile all experimental data.

EXPERIMENTAL PROCEDURES

Materials—[^{3}H]Quinuclidinyl [*phenyl*-4-^{3}H]benzilate (42 Ci/mmol; [^{3}H]QNB) and [*N-methyl*-^{3}H]scopolamine (81 Ci/mmol; [^{3}H]NMS) were from PerkinElmer Life Sciences. Pirenzepine dihydrochloride, atropine sulfate, and carbachol chloride were supplied from Sigma. Bodipy (558/568) pirenzepine dihydrochloride was from Invitrogen.

Expression of Chimeric hM1 Receptors in HEK 293 Cells—The human M1 muscarinic receptor with a truncated N terminus fused to EGFP, referred to as EGFP(Δ17)hM1, was designed and expressed in HEK 293 cells as reported previously (22). Cells were grown in minimal essential medium (Invitrogen) complemented with 10% fetal calf serum, 2 mM glutamine, and antibiotics. Receptor expression levels were assessed from saturation binding experiments, performed under equilibrium conditions for [^{3}H]NMS (4 h at 20 °C) or [^{3}H]QNB (90 min at 37 °C) binding to EGFP(Δ17)hM1-expressing cells (22, 24).

Incubation proceeded in HEPES/BSA buffer (10 mM HEPES, 137.5 mM NaCl, 1.25 mM $MgCl_2$, 1.25 mM $CaCl_2$, 6 mM KCl, and 10 mM glucose, pH 7.4, supplemented with 1 mg/ml bovine serum albumin). Mean values for apparent equilibrium dissociation constants (K_d) and maximal densities (B_{max}) in receptor sites were 95 pM and 590 fmol/10^6 cells ([^{3}H]NMS) and 75 pM and 700 fmol/10^6 cells ([^{3}H]QNB), respectively.

Steady-state FRET Monitoring of Bodipy-Pirenzepine Binding to EGFP(Δ17)hM1 Receptors—Steady-state fluorescence data were acquired on a Spex 2 spectrofluorimeter (HORIBA Jobin Yvon), using intact cells as described (22), with few modifications.

EGFP(Δ17)hM1 cells were suspended in HEPES/BSA buffer (typically at 2×10^6 cells/ml; 1 nM receptor concentration), placed in a quartz cuvette with magnetic stirring, and maintained at 20 °C in a thermostated holder to avoid possible artifacts because of receptor internalization. Fluorescence emission at 510 nm was collected every 0.25 s from cells excited at 470 nm. Time-based recordings of fluorescence intensity started with addition of 4 μl of BoPz (250-fold concentrated stock solution in DMSO) to the 1-ml cell suspension and were pursued until binding equilibrium.

Experiments were carried out over a wide range of ligand concentrations (4–400 nM), corresponding to a 4–400 molar excess over the M1 receptor concentration and 0.4–40-fold the K_d value reported for BoPz binding at EGFP(Δ17)hM1 receptors (22, 23). Dissociation of ligand-receptor complexes was initiated by the addition of 10 μM atropine to the incubation medium (at given time points of the ongoing association process or after BoPz binding equilibrium completion) and followed in real time as described above.

Changes in fluorescence emission at 510 nm as a function of time were first analyzed by nonlinear fitting of individual traces to a two-exponential model: $F(t) = a_0 + a_1 \cdot e^{-k_{app,1} \times t} + a_2 \cdot e^{-k_{app,2} \times t}$, where a_1 and a_2 are the fluorescence changes associated with the two phases, a_0 is the fluorescence intensity at infinite time, $k_{app,1}$ and $k_{app,2}$ are the apparent rate constants (in s^{-1}) for the two phases, and t is the time. In a second step, the sets of progress curves were simultaneously analyzed with the DYNAFIT (3.28 version) numerical resolution software (BioKin Ltd.). Best fit values of the unknown parameters were calculated using the Levenberg-Marquardt algorithm (25). Numerical tests (Kolmogorov, Durbin-Wattson, Tukey statistics) and the reduced χ^2 values were used to evaluate goodness of fit.

Time-resolved Fluorescence Measurements—Time-resolved measurements were performed on EGFP(Δ17)hM1 cell suspensions, using the TCSPC technique, as described previously (28, 29). Excitation pulses at 470 nm were provided by a pulse-picked frequency-doubled Ti:Sapphire laser (Tsunami, Spectra-Physics) pumped by a Millenia X laser (Spectra-Physics). Emission was collected through a polarizer set at magic angle and an 8-nm bandpass H10 monochromator (HORIBA Jobin Yvon) at 510 nm. The instrumental response function was recorded with a polished aluminum reflector, and its full width at half-maximum was 40 ps. All data were collected in the precount mode (500,000 counts per run) to get statistically relevant distribution analyses of donor lifetime species, independent from the fluorescence levels of cell samples. Decays were analyzed using the maximum-entropy method and the Pulse 5 software (30).

Nontransfected cells and EGFP(Δ17)hM1-expressing cells were suspended in HEPES/BSA buffer at a density of 2×10^6 cells/ml. 1 ml of cell suspension (preincubated or not with various unlabeled ligands) was introduced into a quartz cuvette, maintained at 20 °C under constant agitation. Vehicle (DMSO) or Bodipy-pirenzepine (4-μl aliquots of various stock solutions) was added to the cell suspension, and sequential lifetime determinations were performed until binding equilibrium. They usually consisted in series of three consecutive acquisition runs separated by varying time intervals, with the sample being kept in the dark. Acquisition times (70–180 s to get 500,000 counts) depended on the sample fluorescence intensity, although time intervals were adjusted according to BoPz concentration and binding kinetics at 20 °C.

FRET efficiency (E) was calculated as follows: $E = {R_0}^6/({R_0}^6 + R^6) = 1 - (\tau_{DA}/\tau_D)$, where R_0 is the Förster radius, R is the actual donor-acceptor distance, and τ_D and τ_{DA} are the donor lifetime in the absence or the presence of acceptor, respectively. Using E, the donor-acceptor separation (R) was determined following $R = R_0\ (1/E - 1)^{1/6}$, with R_0 taken as 49.7 Å for the EGFP/Bodipy pair (22).

Fluorescence Correlation Spectroscopy—FCS measurements were performed on a home-built setup (26, 27). Two-photon excitation at 900 nm was provided by a mode-locked Ti:Sapphire laser (Tsunami, Spectra Physics). Photons were detected with an Avalanche Photodiode (APD SPCM-AQR-14-FC,

PerkinElmer Optoelectronics), and the normalized autocorrelation function $G(\tau)$ was calculated on line using a hardware correlator (ALV 5000, ALV GmbH).

Adherent HEK 293 cells, with stable expression of EGFP(Δ17)hM1 receptors, were seeded at low density in two-well cover glass chamber slides (Nalge Nunc International) and maintained in phenol red-free culture medium for at least 12 h before the experiment. Prior to data acquisition, the medium was changed to HEPES/BSA buffer, supplemented or not with 10 μM pirenzepine, and cells were allowed to incubate for 30 min at 20 °C.

A similar preparation was applied to HEK cells with transient expression of glycosylphosphatidylinositol (GPI)-anchored EGFP. A pEGFP-N1 plasmid (Clontech) encoding for an EGFP with an endoplasmic reticulum import signal and a GPI anchor signal, fused at its N- and C-terminal ends, respectively, was kindly provided by Dr. P. Keller (Dresden, Germany). Cells were transfected with the plasmid (48 h before FCS analyses) using Lipofectamine™ 2000 according to manufacturer's instructions (Invitrogen).

FCS measurements consisted of multiple runs (40) of short duration (5 s) applied to each specific position selected on the cell plasma membrane. The excitation power was about 3 milliwatts at the sample level. Such conditions have been found optimal to overcome the inherent heterogeneity of the cellular membrane (no real steady state for the fluorescence intensity fluctuations) and to minimize probe photobleaching (31).

FCS autocorrelation curves were individually fitted with the standard two-dimensional diffusion model as follows: $G(\tau) = (1/N) \times (1 + \tau/\tau_D)^{-1} + B$, where N is the average number of fluorescent species in the focal volume, τ the lag time, τ_D the average residence time in the focal volume, and B an offset. The experimental curves were analyzed with an Igor Pro (Wavemetrics) function written to automatically process the data.

The molecular brightness of the fluorescent species diffusing through the excitation volume is defined as the number of photons emitted by a particle/s for a given excitation intensity. This parameter was obtained by dividing the average fluorescence intensity $\langle F \rangle$ by the average number (N) of fluorescent species in the focal volume for each individual curve (5-s acquisition).

The point spread function (*i.e.* focal volume) of the setup was determined from a z-scan on one fluorescein-labeled bead (diameter 20 nm). The measured lateral (0.34 μm) and axial (1.1 μm) resolutions defined an excitation volume of 0.2 fl.

The system was calibrated with 50 nM tetramethylrhodamine (TMR). Assuming a diffusion constant $D_{TMR} = 2.8 \times 10^{-10}$ $m^2 \cdot s^{-1}$ for TMR (32), the diffusion constant D_r for the EGFP(Δ17)hM1 receptors was calculated using $D_r = D_{TMR} \times \tau_{D,TMR}/\tau_{D,R}$, where $\tau_{D,TMR}$ and $\tau_{D,R}$ are the average diffusion times in the focal volume of TMR and EGFP-fused receptors.

RESULTS

Steady-state Fluorescence Monitoring of BoPz Binding to EGFP(Δ17)hM1 Receptors—Real time monitoring of steady-state FRET signals from EGFP(Δ17)hM1 cell suspensions with increasing BoPz concentrations was undertaken to get fine kinetic insights into the interaction of this fluorescent pirenzepine derivative with the M1 receptor (Fig. 1). We observed (Fig. 1*A*) a time-dependent and ligand concentration-dependent decrease in EGFP fluorescence that reaches a maximal amplitude (FRET signal close to 45%) at saturating ligand concentrations. As BoPz binding time courses displayed a marked biphasic behavior, we first adopted an empirical two-exponential model to fit the association traces over the entire ligand concentration range. Individual curve fitting led, for each tested BoPz concentration, to a set of amplitudes (a_1 and a_2) and of apparent rate constants ($k_{app,1}$ and $k_{app,2}$) for a fast and a slow binding component, respectively.

Analysis of the fast step (Fig. 1*B*) indicates a linear relationship of the $k_{app,1}$ values with the ligand concentration, in line with a simple bimolecular Reaction 1,

$$L + R \underset{k_{-1}}{\overset{k_1}{\rightleftharpoons}} RL^*$$

REACTION 1

Under pseudo-first order conditions, the apparent rate constant is given by $k_{app,1} = k_{-1} + k_1 \times [L]$. This allowed us to calculate the association k_1 ($2.18 \pm 0.12 \times 10^5$ $M^{-1} \cdot s^{-1}$) and dissociation k_{-1} (0.025 ± 0.002 s^{-1}) rate constant values (mean values ± S.E.; $n = 4$).

The slow binding process is characterized by a hyperbolic dependence of the $k_{app,2}$ values with ligand concentration (Fig. 1*C*), in line with a two-step binding process, as shown in Reaction 2,

$$L + R \underset{k_{-1}}{\overset{k_1}{\rightleftharpoons}} RL^* \underset{k_{-2}}{\overset{k_2}{\rightleftharpoons}} RL$$

REACTION 2

where a fast bimolecular binding event is followed by a rate-limiting conversion of the RL* complex into a higher affinity RL state. The time course for this reaction is defined by $k_{app,2} = k_{-2} \times ([L]/([L] + K_1)) + k_{-2}$, where k_2 is the forward and k_{-2} the backward rate constant of the interconversion between RL* and RL complexes, and K_1 is the equilibrium dissociation constant for the intermediate RL* complex. Nonlinear least square fitting of data (Fig. 1*C*) to this equation yielded $k_2 = 8.8 \pm 0.4 \times 10^{-3}$ s^{-1}, $k_{-2} = 0.55 \pm 0.03 \times 10^{-3}$ s^{-1}, and $K_1 = 111 \pm 7$ nM (mean values ± S.E.; $n = 4$).

Fig. 1*D* shows that the variation with BoPz concentration of the overall FRET signal defines, as expected, a typical saturation isotherm with a K_d value (12 ± 1 nM; mean ± S.E.; $n = 4$), and a maximal fluorescence extinction (44%; taken here as 100% of the FRET signal at equilibrium) in good agreement with previous data (22, 23). Interestingly, the examination of the fluorescence changes associated with the rapid (a_1 values) and slow (a_2 values) binding components (Fig. 1*D*) pointed to the high contribution to the overall FRET signal of the fast binding component (more than 80% at infinite BoPz concentrations) and the bell-shaped dependence with ligand concentration of the slow component. Both observations are clearly inconsistent with Reaction 2 and indicate that a more complicated binding model applies.

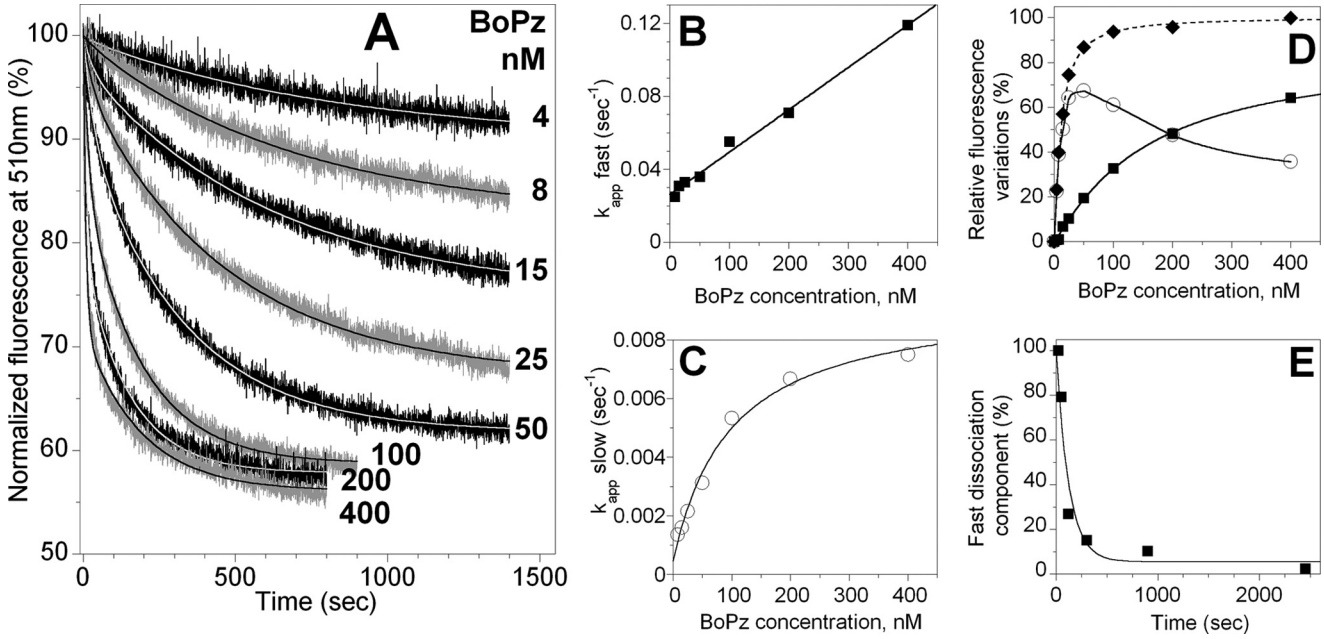

FIGURE 1. **Real time recordings of BoPz binding to EGFP(Δ17)hM1 receptors and experimentally derived parameters.** *A,* time course of BoPz interaction with EGFP(Δ17)hM1 receptors at 20 °C. Fluorescence at 510 nm (excitation set at 470 nm) was recorded (data acquisition every 0.25 s) from cell suspensions (2×10^6 cells/ml) mixed with BoPz (added at time 0) at the indicated final concentrations. Fluorescence is normalized to the intensity in the absence of ligand. *Solid lines* are best fits to a two-exponential model. *B,* plot of the apparent rate constant ($k_{app,1}$, determined from trace fitting in *A*) for the fast (■) binding step *versus* BoPz concentration. Onward k_1 and backward k_{-1} rate constants were, respectively, 2.32×10^5 $M^{-1} \cdot s^{-1}$ and 26×10^{-3} s^{-1}. *C,* plot of the apparent rate constant ($k_{app,2}$, determined from trace fitting in *A*) for the slow (○) binding step *versus* BoPz concentration. Onward k_2 and backward k_{-2} rate constants were, respectively, 9×10^{-3} and 0.68×10^{-3} s^{-1}. *D,* relative contributions of the rapid (■) and slow (○) binding steps to the overall FRET signal (◆) at equilibrium. Binding component amplitudes are from two exponential fit of traces in *A*, normalized to maximal fluorescence extinction measured at saturating concentrations of BoPz at equilibrium. *E,* effect of incubation duration on fast BoPz dissociation at 10 °C. Incubation started with the addition of 100 nM BoPz to the cell suspension and proceeded for various periods of time (20–2500 s) until dissociation was promoted by the addition of 10 μM atropine. Fluorescence emission was further recorded until full recovery. Biphasic dissociation traces fitted a sum of two exponentials, with a fixed pair of rate constants (set at 0.015 and 0.0003 s^{-1}) and variable amplitudes. Relative amplitudes for the rapid recovery phase (■) are plotted as a function of incubation time, and the best mono-exponential fit to the data is shown (rate constant: $8 \pm 2 \times 10^{-3}$ s^{-1}).

Finally, dissociation experiments were undertaken at 10 °C (to slow down overall reaction rates) by adding the antagonist atropine in excess (10 μM) at different time points after mixing BoPz (100 nM) with the cell suspension. Two categories of ligand-receptor complexes were identified with fast (0.015 s^{-1}) and slow (3×10^{-3} s^{-1}) off-rates.

As shown in Fig. 1*E*, the proportion of the fast reversible binding component decreases with the prolongation of the incubation time according to a monoexponential law. It becomes negligible after a 40-min incubation period, in agreement with a full and homogeneous dissociation of ligand-receptor complexes (23). These results are consistent with a time-dependent interconversion of intermediate complexes into a final higher affinity one.

Taken together, these steady-state data suggest a binding model that involves more than one intermediate receptor state. Time-resolved FRET measurements were then undertaken to identify and quantify individual EGFP-labeled receptor species involved in BoPz binding.

Time-resolved Measurements on EGFP(Δ17)hM1-expressing Cell Suspensions—With a high photon counting rate and good statistics, the TCSPC technique offers the possibility to dissect up to five lifetime components with temporal resolution down to 20 ps.

Fig. 2 shows typical fluorescence decay curves for nontransfected HEK cells and EGFP(Δ17)hM1-expressing cells (both taken at an identical density of 2×10^6 cells/ml), in the absence or the presence of BoPz. The corresponding lifetime distribution patterns, with lifetime values (τ), amplitudes (α), and relative contribution (f) to overall intensity, are given in Table 1.

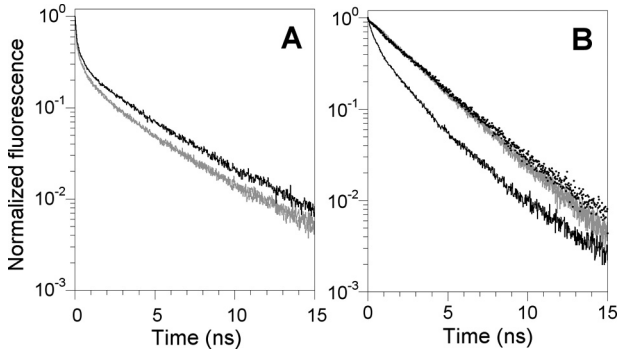

FIGURE 2. **Typical fluorescence decay curves for nontransfected HEK and EGFP(Δ17)hM1 cells.** Fluorescence decays were recorded from HEK (*A*) and EGFP(Δ17)hM1 (*B*) cell suspensions, in the absence of ligand (*gray traces*) or after preincubation for 30 min in the presence of 300 nM BoPz (*black traces*) or 300 nM Bodipy (558/568) (*dots*). Because of the low fluorescence of HEK cells, acquisition times for decays in *A* were at least 10 times longer than in *B*. Time-resolved parameters corresponding to best fits to these data are summarized in Table 1.

Nontransfected HEK cells (Fig. 2*A*) exhibit a biexponential decay, with a major τ_1 component at 0.13– 0.16 ns and a second one, τ_2, at 1.3–1.8 ns, that probably reflect the diversity of components involved in cell autofluorescence. The fluorescence level of nontransfected HEK cells was at least 10 times lower than that of M1 receptor-expressing ones at the same density,

indicating negligible contribution of autofluorescence in the decays of EGFP(Δ17)hM1 cells.

EGFP(Δ17)hM1-expressing cells (Fig. 2*B*), in the absence of ligand, also display a biexponential lifetime profile with a minor short lived τ_1 component at 0.22–0.25 ns (cell autofluorescence) and a dominant long lived lifetime species at 2.56 ns, characteristic for unquenched EGFP (33, 34). When BoPz (300 nM) was added and allowed to reach equilibrium with EGFP(Δ17)hM1 receptors, the lifetime pattern exhibited profound variations as follows: (*a*) an important decrease in the $\langle\tau_m\rangle$ value, indicating an efficient energy transfer ($E \sim 0.57$) from the EGFP donor to the Bodipy acceptor fluorophores; (*b*) a dramatic decrease (90 to 20%) in the amplitude of the long lived τ_3 species representative of free receptors; (*c*) an increased contribution of the short lived τ_1 component, which now significantly participates to the overall fluorescence intensity; (*d*) the appearance of an additional lifetime species, with an intermediate τ_2 value at 1.2 ns.

The addition of BoPz (300 nM) to HEK cells (Fig. 2*A*) or of the Bodipy (558/568) fluorophore alone (300 nM) to EGFP(Δ17)hM1 cells (Fig. 2*B*) marginally affected the fluorescence decays for these cells. The only significant feature was the appearance of a minor long lived component ($\tau = 4.6 \pm 0.3$ ns) that coincided well with the excited state lifetime values reported for Bodipy fluorophores (35). As this minor species likely arises from direct excitation of the acceptor at 470 nm, it was ignored in all subsequent lifetime distributions to focus only on EGFP lifetime species.

Evidence for Ligand-induced and Receptor-driven EGFP Lifetime Species Redistribution—Several controls were performed to ascertain the receptor specificity of the variations in τ species (and associated populations) for EGFP(Δ17)hM1 cells in the presence of BoPz (Table 2). Addition of a saturating (10 μM) concentration of atropine (a prototypical muscarinic antagonist), prior to BoPz, left the lifetime pattern of cells unchanged. Thus, the strong FRET signal is specifically due to the interaction of BoPz with the muscarinic M1 receptor.

We next addressed the origin of the fractional increase in the amplitudes of both τ_1 and τ_2 species in the presence of BoPz. Short lifetimes for EGFP have been previously linked to its protonated form, which exhibits an excitation maximum at 400 nm (36, 37). Although these studies pointed to the weak pH sensitivity of the EGFP lifetime at 488 nm, one cannot exclude that a fraction of protonated EGFP state might be excited at 470 nm. Thus, variations in the amplitudes of the short lived species could stem from EGFP-fused receptors trapped into acidic endosomes, as a consequence of ligand-promoted receptor internalization. Receptor endocytosis is usually regarded as an agonist-driven phenomenon hard to reconcile with the use of BoPz, a muscarinic antagonist derivative. Nevertheless, to address this issue, experiments were performed at 20 °C on EGFP(Δ17)hM1 cells pretreated either with 100 μM carbachol, a typical muscarinic agonist, or with 0.4 M sucrose, a blocker of clathrin-mediated internalization (38). None of these treatments significantly affected the values or the relative amplitudes of the lifetime components (Table 2), indicating that, in our conditions, M1 receptor internalization was negligible and/or did not involve acidification of the EGFP environment. Thus, increased proportions of τ_1 and τ_2 species are relevant signals arising from specific BoPz binding to M1 receptors.

Finally, we questioned the origin of the residual (20–25%) long lived τ_3 species that systematically persisted at M1 receptor saturation (Tables 1 and 2). A plausible explanation considering the existence of intracellular EGFP-fused receptor sites, inaccessible to BoPz, was confirmed in two ways. First, comparison of B_{max} values for [^{3}H]NMS binding (at 20 °C) to cell surface receptors and for [^{3}H]QNB binding (at 37 °C) to total cell receptor sites indicated that the more hydrophilic [^{3}H]NMS

TABLE 1

Fluorescence decay parameters for nontransfected and EGFP(Δ17)hM1-expressing cells before and after BoPz binding equilibrium

Fluorescence decays were collected from nontransfected HEK cells and from EGFP(Δ17)hM1-expressing cell suspensions, preincubated for 30 min at 20 °C in buffer alone or in the presence of a 300 nM saturating BoPz concentration. Mean values and associated standard errors for the amplitudes α_i and lifetimes τ_i are from independent determinations on HEK cells ($n = 3$) and on EGFP(Δ17)hM1-expressing cell lines originating from various transfection and selection steps ($n = 3$–5). $\langle\tau_m\rangle$ corresponds to the mean lifetime, with $\langle\tau_m\rangle = \Sigma\ \alpha_i\ \tau_i$. The contribution f_i of each species to the overall fluorescence intensity is calculated with $f_i = \alpha_i\ \tau_i/\langle\tau_m\rangle$.

Parameter	HEK cells		EGFP(Δ17)hM1 cells	
	Buffer	+ BoPz	Buffer	+ BoPz
τ_1 (ns)	0.13 ± 0.03	0.16 ± 0.01	0.22 ± 0.09	0.25 ± 0.08
α_1 (%)	89 ± 5	85 ± 9	10 ± 1	47 ± 4
f_1 (%)	44	34	1	12
τ_2 (ns)	1.3 ± 0.5	1.8 ± 0.6		1.2 ± 0.1
α_2 (%)	11 ± 5	15 ± 9		33 ± 2
f_2 (%)	56	66		38
τ_3 (ns)			2.56 ± 0.06	2.53 ± 0.03
α_3 (%)			90 ± 1	20 ± 3
f_3 (%)			99	49
$\langle\tau_m\rangle$ (ns)	0.26	0.40	2.32	1.00

TABLE 2

Pharmacological evaluation of the receptor specificity of lifetime species redistribution upon BoPz binding to EGFP(Δ17)hM1 cells

EGFP(Δ17)hM1 cell suspensions were preincubated in the absence (control) or the presence of either atropine (10 μM; 30 min), carbachol (100 μM; 1 h), or sucrose (0.4 M; 30 min). Thereafter, BoPz was added at a final 300 nM concentration, when indicated, and allowed to equilibrate for 25 min at 20 °C. Fluorescence decays were acquired and analyzed as described under "Experimental Procedures." Lifetime species and amplitudes (mean values ± S.E. for triplicates) are expressed as reported in Table 1.

Lifetime parameters	Control		Atropine		Carbachol	Sucrose	
	None	+ BoPz	None	+ BoPz	None	None	+ BoPz
τ_1 (ns)	0.14 ± 0.02	0.23 ± 0.04	0.24 ± 0.07	0.30 ± 0.11	0.16 ± 0.03	0.15 ± 0.02	0.20 ± 0.01
α_1 (%)	10 ± 1	42 ± 0.3	14 ± 2	12 ± 1	8 ± 1	15 ± 1	44 ± 1
τ_2 (ns)		1.22 ± 0.04					1.17 ± 0.09
α_2 (%)		34 ± 3					33 ± 5
τ_3 (ns)	2.54 ± 0.02	2.40 ± 0.01	2.59 ± 0.03	2.60 ± 0.07	2.43 ± 0.02	2.35 ± 0.01	2.39 ± 0.13
α_3 (%)	90 ± 1	24 ± 3	86 ± 2	88 ± 3	92 ± 1	85 ± 2	23 ± 3%
$\langle\tau_m\rangle$ (ns)	2.31	1.09	2.21	2.32	2.24	2.01	1.02

radioligand labeled only 80–85% of the total receptor population. Second, taking advantage of the exquisite pH dependence ($pK_a = 6$) of EGFP fluorescence (36), we found that the fluorescence at 508 nm of EGFP(Δ17)hM1 cells was instantaneously quenched by 75–80% through acidification, pH 5, of the extracellular milieu, whereas membrane permeabilization was required to abolish the residual EGFP emission.

All these data highlight the reproducibility, receptor specificity, and sensitivity of TCSPC measurements on living cell suspensions. Thus, the FRET signal arising from BoPz binding to EGFP-fused M1 receptors could be solved into τ_1 and τ_2 lifetime species, representative of ligand-receptor complexes. Assuming mean values (in ns; $n = 6$) of 0.24 ± 0.01, 1.21 ± 0.04, and 2.46 ± 0.03 for τ_1, τ_2, and τ_3 (free receptors) species, respectively, FRET efficiency and donor-acceptor separation for the ligand-receptor complexes associated with τ_1 and τ_2 lifetimes were calculated (as reported under "Experimental Procedures"). With an efficiency of 0.90 ± 0.01, the τ_1 lifetime component reports on a close EGFP-Bodipy proximity (R = 34.4 ± 0.6 Å), whereas the τ_2 species, with an efficiency of 0.50 ± 0.01, points to a more distant donor-acceptor interaction (R = 49.7 ± 0.6 Å), close to the average 45.4 Å distance previously determined from steady-state FRET experiments (22, 23).

Interestingly, the τ_1 and τ_2 species are consistent with the tandem two-site model (21), according to which a ligand may translocate from a peripheral to a more central receptor-binding site. With EGFP facing the extracellular milieu, occupation of the peripheral site by BoPz is thus expected to feature a shorter interchromophore distance (and a shorter lifetime value) than occupation of a deeper receptor site.

Time Dependence of BoPz-induced EGFP Lifetime Distribution—The redistribution of EGFP lifetime species consecutive to BoPz binding was examined as a function of ligand association time (Fig. 3).

Lifetime decay measurements started with ligand addition to the cell suspension and were repeated at a frequency compatible with the collection of 500,000 counts/decay. Such conditions were essential to get relevant determinations of multiple lifetimes but precluded fine kinetic analyses for initial binding steps, especially at BoPz concentrations >50 nM.

We first verified that the relative amplitudes (α_1 and α_3 values) of the two characteristic components detected in the absence of ligand were stable over time. Fig. 3 also shows that the addition of 50 nM BoPz promoted the appearance of the τ_2 lifetime species together with a time-dependent redistribution of the amplitudes associated with the three lifetime species. Importantly, all lifetime values remained constant over time and did not vary significantly upon ligand addition. As expected for a binding process viewed as an energy transfer-mediated EGFP donor extinction, the amplitude of the long lived τ_3 species decreases with time, reaching a plateau at equilibrium time. This confirms that the τ_3 species is characteristic of free EGFP-fused M1 receptors, whereas τ_1 and τ_2 lifetime components depict different ligand-receptor complexes. Interestingly, the population of τ_1 species increased faster than that of τ_2 ones, suggesting a sequential process in line with an initial binding step to a peripheral receptor site followed by ligand translocation (21). However, at variance with the expectations for a simple interconversion process, the increase in the amplitude of the τ_2 lifetime component was not accompanied with a concomitant decrease in τ_1 lifetime amplitude. It was thus tempting to consider that an additional ligand-receptor complex, endowed with a similar τ_1 lifetime value, slowly accumulated with time.

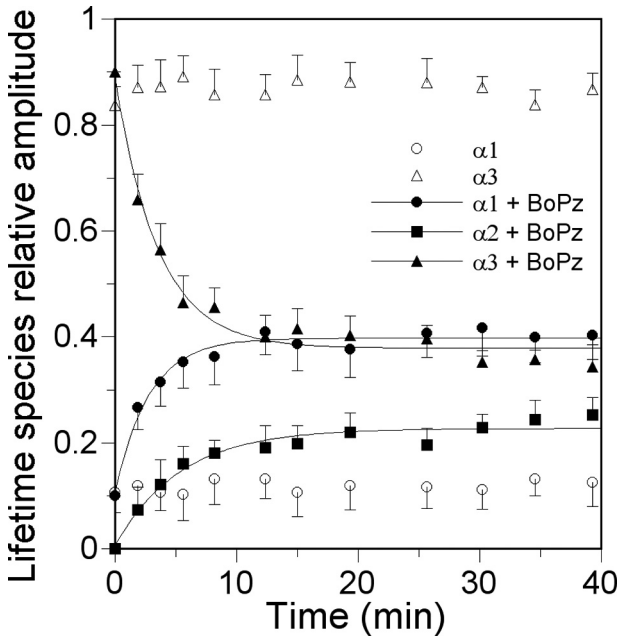

FIGURE 3. **Time-dependent changes in the amplitudes of lifetime species upon BoPz addition to EGFP(Δ17)hM1 cells.** Fluorescence decays were recorded from cell suspensions, maintained at 20 °C, at selected times following BoPz (50 nM) addition. The relative amplitude α_1 (●), α_2 (■), and α_3 (▲) values, respectively, associated to the τ_1, τ_2, and τ_3 lifetime species that were identified, are plotted as a function of BoPz incubation time. Mean amplitude values and associated standard deviations for two separate experiments are shown. As a control, the amplitudes for the short (○) and the long lived (△) species, observed in the absence of ligand, were recorded under the same conditions. Lifetime values (in nanoseconds) remained stable over the whole experiment, BoPz being present or not ($\tau_1 = 0.23 \pm 0.04$; $\tau_2 = 1.18 \pm 0.06$; $\tau_3 = 2.54 \pm 0.05$; mean values ± S.E.; $n = 23$).

Evidence for Ligand-induced Muscarinic Receptor Dimerization—Ligand-bound receptor homodimers may be regarded as possible candidates for additional short lived lifetime species. Indeed, there is a growing body of evidence for GPCRs (and muscarinic receptors) to exist as constitutive or ligand-inducible dimers (39–41). Moreover, the occurrence of both intra- and inter-subunit energy transfer in such BoPz-EGFP(Δ17)hM1 dimers is expected to promote a strong FRET signal, compatible with the τ_1 lifetime value.

FCS was selected as an appropriate method to test the dimerization hypothesis. It records fluorescence intensity fluctuations of molecules crossing a small two-photon excitation volume. It allows the determination of the diffusion coefficient, the average number, and the individual molecular brightness (the product of the molecular extinction coefficient by the quantum yield of fluorescence and the detection efficiency of the microscope) of diffusing particles in living cells (42, 43). In our particular case, brightness analysis was of special interest, as conversion of a fluorescent molecule from a monomeric to a dimeric state (*i.e.* a particle which carries two fluorophores) is expected to increase this parameter by a factor of 2 (44).

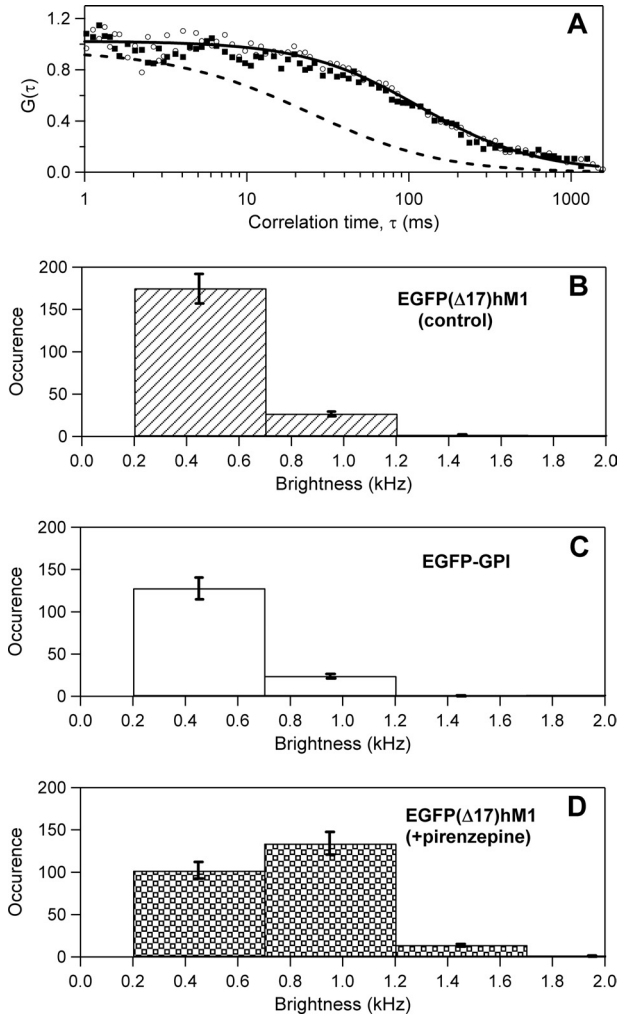

FIGURE 4. **Two-photon FCS experiments on EGFP(Δ17)hM1 receptors and EGFP-GPI expressed in HEK 293 cells.** *A,* autocorrelation curves of EGFP(Δ17)hM1 cells in the absence (○) and the presence (■) of 10 μM unlabeled pirenzepine are shown together with their fits (*solid line*). The autocorrelation curve of free EGFP molecules (100 nM) in pure glycerol (*dotted line*) was fitted with the standard three-dimensional diffusion model, giving a diffusion coefficient of $9 \pm 0.2 \times 10^{-9}$ cm^2·s^{-1}. *B,* brightness distribution of EGFP(Δ17)hM1 receptors in the absence of ligand (control). *C,* brightness distribution of EGFP-GPI. *D,* brightness distribution of EGFP(Δ17)hM1 receptors after a 30-min incubation of the cells in the presence of 10 μM pirenzepine. The *histograms* were obtained by sorting the measured brightness values ($n \approx 200$) into different classes of 0.5 kHz in width to account for the individual brightness of EGFP molecules. The occurrence represents the number of events displaying a brightness value composed between x and $x + 0.5$ kHz. Events below a 0.2 kHz threshold, likely reflecting fluorescence background, were not considered. The *error bars* take into account the uncertainty for the measurement of the number of molecules (N) within the focal volume.

FCS experiments were undertaken on adherent EGFP (Δ17)hM1 cells, using unlabeled antagonist pirenzepine (Pz) as the ligand. First, in the absence of ligand (Fig. 4*A*), the autocorrelation function $G(\tau)$ indicates a slow diffusion ($2.5 \pm 0.7 \times 10^{-9}$ cm^2·s^{-1}), homogeneous all over the plasma membrane (and in different cells) and fully consistent with values (1 to 4×10^{-9} cm^2. s^{-1}) reported for several GPCRs in various cell hosts (Refs. 45, 46 and references therein). The distribution of EGFP-fused M1 receptor brightness (Fig. 4*B*), established from a large number of measurements ($n \approx 200$) at the cell plasma membrane level performed in the absence of ligand, is nearly monodisperse and centered at about 0.45 kHz.

To take into account the unavoidable photobleaching of slowly moving membrane proteins (12, 31), this brightness value was first compared with that of free EGFP molecules diffusing with comparable rates in a viscous medium. In glycerol, purified EGFP molecules exhibit a brightness value (0.4 kHz) very close to that of EGFP(Δ17)hM1 receptors. This represents a strong argument in favor of a monomeric state for the receptors. Indeed, earlier work (47, 48) reported that purified EGFP molecules behave as monomers in aqueous solution and that EGFP brightness is a robust parameter to study oligomerization processes in cells, independent on the concentration and the cellular environment of the fluorescent protein.

We used HEK cells expressing an EGFP fused to a GPI-attachment signal (49) as an additional control. Indeed, this protein and other GPI-fused GFP variants were found to behave as plasma membrane protein markers (49) and to reside there essentially as monomers (50). Transient expression of EGFP-GPI into HEK cells was accompanied with fluorescence nicely delineating the cell contour, reflecting GPI-mediated anchoring of EGFP at the plasma membrane surface (49).

Examination of these cells through FCS allowed the determination of a diffusion coefficient ($2.9 \pm 0.6 \times 10^{-9}$ cm^2·s^{-1}) close to that of EGFP(Δ17)hM1 receptors. The brightness profile of EGFP-GPI species (Fig. 4*C*) exhibited a major population, with a brightness centered at about 0.45 kHz, and a minor one (20%) with double brightness. These findings nicely meet previous conclusions drawn from homo- and hetero-FRET studies, revealing that GPI-anchored GFP variants predominate as monomers (50). All these controls support that EGFP(Δ17)hM1 receptors, in the absence of ligand, exhibit a brightness similar to that of monomeric EGFP, either soluble or membrane-bound.

Most interestingly, in the presence of 10 μM pirenzepine (Fig. 4*D*), a receptor population with a brightness centered around 0.9 kHz predominates, in line with ligand-induced dimerization of the M1 receptors. This process is not complete as a significant proportion of monomeric receptors (with a 0.45 kHz brightness) still exists in the presence of Pz. Species with higher brightness, which probably correspond to higher order oligomeric states, are negligible. As shown on Fig. 4*A*, the diffusion coefficient does not significantly change upon addition of Pz ($3.0 \pm 0.5 \times 10^{-9}$ cm^2·s^{-1}). This was not unexpected, as a 2-fold increase in mass (dimerization) has a poor impact on the diffusion coefficient of proteins in biological membranes (43, 51). Finally, it is important to mention that receptor homodimerization does not result from an artificial protein-protein association driven by EGFP self-aggregation or crowding effects (Fig. 4*B*) and that truncation of the M1 receptor N terminus, and its fusion to EGFP, does not hinder receptor dimerization (Fig. 4*D*).

Toward a Binding Model—The following model (Reactions 3 and 4), based on experimental information provided by steady-state and time-resolved fluorescence spectroscopy and by the FCS study, was proposed to describe BoPz binding to EGFP(Δ17)hM1 receptors,

$$L + R \underset{k_{-1}}{\overset{k_1}{\rightleftharpoons}} RL^* \underset{k_{-2}}{\overset{k_2}{\rightleftharpoons}} RL$$

REACTION 3

and

$$RL + RL \underset{k_{-3}}{\overset{k_3}{\rightleftharpoons}} R_2L_2$$

REACTION 4

In this model, an initial bimolecular recognition step is followed by a conversion of the intermediate RL* complex into a higher affinity RL state that, upon dimerization, leads to the final R_2L_2 complex.

This model was described in a set of differential equations (integrating all predicted rate constants and concentrations of receptor states; see the supplemental material) and in corresponding intensity Equation 1,

$$I = I_0\frac{R}{Rt} + I_1\frac{RL^*}{Rt} + I_2\frac{RL}{Rt} + 2I_1\frac{R_2L_2}{Rt} + I_3 \qquad \text{(Eq. 1)}$$

in which the intrinsic fluorescence intensity for each EGFP-fused receptor species was deduced from lifetime values.

Indeed, as the quantum yield of a fluorophore is directly proportional to its excited state lifetime, the intensity I and lifetime τ values for any given ligand-receptor complex can be calculated as follows: $I/I_0 = \tau/\tau_0$, where I_0 (taken as 1) and τ_0 (the experimentally defined τ_3 value taken as 2.5 ns) specify the intensity and lifetime values for R, the free EGFP-fused receptors. The intrinsic intensity I_1 (0.1) and I_2 (0.48) parameters are thus directly proportional to the experimentally defined τ_1 (0.25 ns) and τ_2 (1.2 ns) lifetime values. As mentioned before, the I_1 intensity was assigned to the initial RL* state and to the R_2L_2 dimer, whereas the I_2 constant was associated to the RL state.

Finally, the fraction of the τ_3 species that did not participate in BoPz binding (intracellular receptor sites) was taken into account, fixing I_3 to 0.2. Thus, in the absence of ligand or at time 0, $[R] = 0.8 \times [R_t]$, where R defines the receptor population "actively" involved in BoPz binding, and R_t indicates the whole cell population of EGFP-fused receptors.

Fig. 5 shows a set of BoPz association traces that were recorded under steady-state FRET conditions and collectively fit using the numerical approach defined above. It may be observed that the dimerization model nicely describes BoPz binding kinetics (χ^2 = 0.9) over a broad ligand concentration range. A permutation in the attribution of the intensity values into Equation 1 was clearly unfavorable (supplemental Table), further validating the selected characteristics of the various complexes in the proposed model. Collective fitting of BoPz binding traces to other models, such as the two-step isomerization and tandem two-site models (supplemental material), either did not converge or was clearly inconsistent (supplemental Table).

Mean rate and equilibrium constant values afforded from numerical resolution of BoPz binding to EGFP(Δ17)hM1 receptors are summarized in Table 3. Parameters for the fast initial bimolecular recognition step allow the estimation of an equilibrium dissociation constant K_1 of 110 nM. The intermediate step that leads to the formation of RL complexes is driven by a K_2 isomerization constant close to 0.1. The third binding step, which promotes the formation of dimers of ligand-receptor complexes (R_2L_2), points to a high affinity of RL monomers for each other (K_3 = 1.7 nM) with a fast association rate. The comparison of K_{dA} and K_{dB} values (the equilibrium dissociation constants for the formation of RL and R_2L_2 complexes, respec-

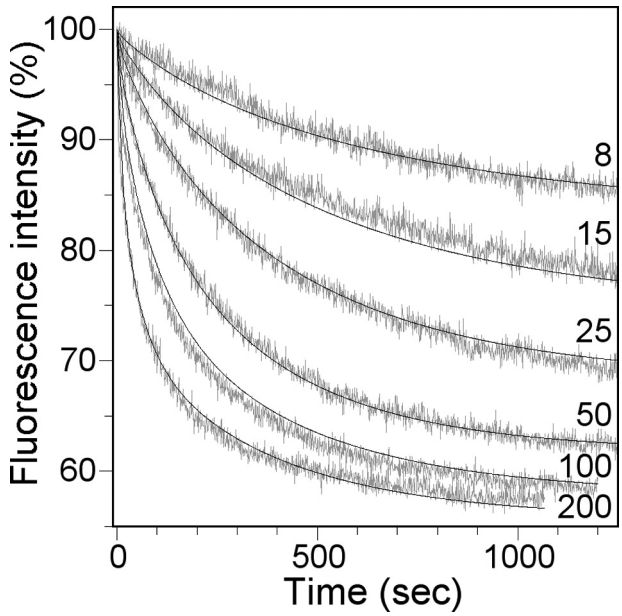

FIGURE 5. **Evaluation of model accuracy to fit BoPz binding kinetics to EGFP(Δ17)hM1 receptors.** A typical series of association traces, recorded under steady-state FRET conditions, was obtained using increasing BoPz concentrations (indicated in nanomolars). Collective fitting of the association traces was performed numerically using the appropriate sets of equations (supplemental material) and intensity constraints (I_0 = 0.8; I_1 = 0.1; I_2 = 0.48; I_3 = 0.2) to integrate information provided by lifetime measurements (see under "Results"). Fit quality was appreciated from the χ^2 value = 0.859.

TABLE 3

Kinetic and equilibrium binding constants for BoPz to EGFP(Δ17)hM1 receptors as afforded from collective fitting of association traces

Numerical resolution of all constants, according to the three-step binding model (Fig. 7), was based on a set of differential equations (supplemental material) and on Equation 1, with constrained intensity values (I_0 = 0.8; I_1 = 0.1; I_2 = 0.48; I_3 = 0.2). Apparent equilibrium dissociation constants K_1, K_2, and K_3 are, respectively, k_{-1}/k_1, k_{-2}/k_2, and k_{-3}/k_3 ratios. K_{dA} values (expressed as the $K_1.K_2$ product) report on the affinity of the RL state, whereas K_{dB} values (expressed as the root square of the $K_1.K_2.K_3$ product) refer to affinity of BoPz-occupied receptor dimers. Mean values and associated standard deviations for two independent experiments are reported together with χ^2 values.

Constants	Mean values
k_1 ($M^{-1}\cdot s^{-1}\cdot 10^5$)	1.4 ± 0.1
k_{-1} ($s^{-1}\cdot 10^{-3}$)	15 ± 1
K_1 (nM)	110 ± 10
k_2 ($s^{-1}\cdot 10^{-3}$)	48 ± 6
k_{-2} ($s^{-1}\cdot 10^{-3}$)	7.6 ± 1.2
K_2	0.16 ± 0.04
k_3 ($M^{-1}\cdot s^{-1}\cdot 10^5$)	13.0 ± 1.5
k_{-3} ($s^{-1}\cdot 10^{-3}$)	2.2 ± 0.5
K_3 (nM)	1.7 ± 0.6
K_{dA} (nM)	17.5 ± 6.0
K_{dB} (nM)	5.5 ± 2.0
χ^2	0.90 ± 0.04

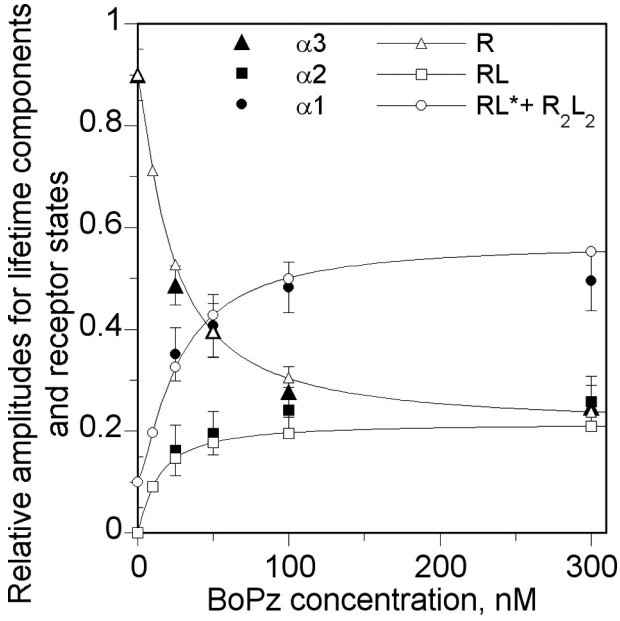

FIGURE 6. **Superimposition of time-resolved amplitudes and of receptor state proportions as predicted by the proposed model for BoPz binding at equilibrium.** Time-resolved studies were performed on EGFP(Δ17)hM1 cells equilibrated with BoPz at various concentrations (25–300 nM). They allowed the experimental determination of the relative α_1 (●), α_2 (■), and α_3 (▲) amplitudes for the short (τ_1, 0.25 ns), intermediate (τ_2, 1.2 ns), and long (τ_3, 2.5 ns) lifetime components, respectively. Mean amplitude values and associated standard deviations for two separate experiments are shown. The theoretical proportions for the various receptor states, as predicted by the proposed binding model, were calculated for each BoPz concentration using a set of differential equations (supplemental material), the intensity constraints ($I_0 = 0.8$; $I_1 = 0.1$; $I_2 = 0.48$; $I_3 = 0.2$), the rate constants listed in Table 3, and an equilibrium time set at 30 min. Calculated receptor state proportions (*open symbols*) and their BoPz concentration dependence (*solid lines*) are as follows: R state (△), RL state (□), and RL* + R_2L_2 states (○).

tively) indicates that dimerization promotes a 3–4-fold enhancement of the affinity for the final BoPz complexes.

To further examine the pertinence of the dimerization model, we compared over a broad range of BoPz concentrations the relative amplitudes at binding equilibrium for the various free and bound receptor states (calculated from the rate constants) with the experimentally defined proportions of τ_1, τ_2, and τ_3 species. This may be regarded as a very stringent test to evaluate model accuracy and propensity to reconcile kinetic and lifetime information provided by independent steady-state and time-resolved measurements. As shown in Fig. 6, the amplitudes of all three lifetime species match well the proportions of the various BoPz-receptor complexes, whatever the ligand concentration. Thus, the proposed binding model was found to reconcile all our data, nicely integrating information from steady-state and time-resolved fluorescence as well as from FCS measurements.

DISCUSSION

Muscarinic acetylcholine receptors (M1–M5 subtypes) are class A GPCRs that bind agonists and competitive antagonists within an orthosteric binding domain, deeply buried in the receptor transmembrane core (15). Their ligand binding properties are essentially from radioligand binding studies, using high affinity antagonists and membrane preparations. At equilibrium, most interactions between muscarinic receptors and

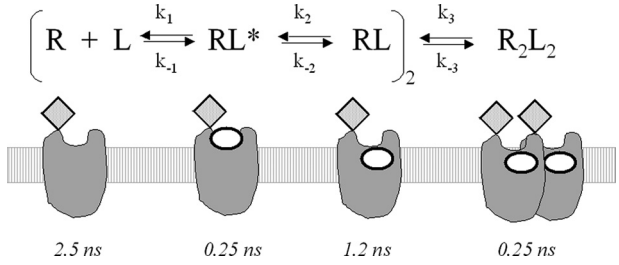

FIGURE 7. **BoPz binding to EGFP(Δ17)hM1 receptors according to the proposed binding model.** A three-step binding mechanism with four receptor states and associated EGFP lifetime species is proposed together with putative locations for the donor (EGFP; *gray diamond*) and acceptor (Bodipy; *oval*) fluorophores.

their competitive antagonists can be interpreted in terms of simple bimolecular reactions, whereas kinetic studies, performed with a variety of tritiated antagonists such as NMS (19), QNB (16–20, 52), *N*-methyl-4-piperidyl benzilate (17, 19), and pirenzepine (52), point to a more complex mechanism. However, because of their poor description of fast binding events, most of these data were consistent with a two-step model wherein fast initial binding is followed by a slow conformational change of the receptor leading to a state that binds the ligand more avidly (receptor isomerization; see Refs. 17, 18, 20). Some of these studies also considered the possibility for two competitive ligands to bind simultaneously to the receptor (53). This question was further addressed on M1 receptors (21), leading to the tandem two-site model where an additional ligand molecule binds with a very low affinity.

Within this context, we monitored (through FRET), in real time and on living cells, the interaction of EGFP-fused M1 receptors with a fluorescent pirenzepine derivative. We evidenced pirenzepine-induced dimerization of the receptors (through FCS) and found that a three-step binding model fully accounted for the experimental data. This model describes (Fig. 7) the formation of a first ligand-receptor complex (RL*) that slowly interconverts into a more stable one (RL), prone to subsequent dimerization (R_2L_2).

The initial RL* complex was associated with a very short lived EGFP lifetime (0.25 ns), indicating an EGFP-Bodipy distance close to 35 Å. Because EGFP is fused to the M1 receptor with a truncated N terminus (three residues away from the receptor TM1 domain; see Ref. 22), such a short distance is an indication for fast initial binding to occur at the outer receptor surface.

In contrast, the tighter RL complex resulting from the slow interconversion step was associated with a significantly higher lifetime value (1.2 ns) and an interchromophore distance close to 50 Å. This unambiguously confirms that, upon BoPz binding, the receptor undergoes a conformational rearrangement that moves the Bodipy group of the bound ligand away from EGFP, mirroring a translocation from a peripheral to a more central receptor site. Thus, these findings support former inferences from radioligand binding studies on muscarinic M1 receptors (21). They also extend pioneering "lifetime" spectroscopic studies on purified β_2-adrenergic receptors, labeled with environmentally sensitive fluorescent probes (54). In this work, the agonist-promoted molecular rearrangements of the β_2-adrenergic receptor contrasted with the poor effects of antagonists, when fluorescein was positioned at the TM_6/i_3 loop interface.

To explain the apparent discrepancy with our results indicating antagonist-driven conformational changes, one may suggest that in the β_2-adrenergic receptor the local rearrangements induced by antagonists do not reach the receptor subdomain probed by fluorescein.

The last step describes the formation of R_2L_2 dimers, associated with a short lived lifetime value that could not be distinguished from that of the "peripheral" RL* complex. Because R_2L_2 results from the association of two RL complexes, with buried ligand molecules, the similarities in the fluorescence lifetimes of R_2L_2 and RL* complexes are probably coincidental. Indeed, the short lifetime value for a dimer of liganded receptors likely stems from both intra-subunit (EGFP and Bodipy bound to the same receptor molecule) and inter-subunit (EGFP fused to one monomer and Bodipy bound to the adjacent receptor molecule) energy transfer. The possibility for a FRET signal to arise from the close proximity of two EGFP molecules was definitively ruled out as follows: (*a*) the signal we monitored (a reduction in donor intensity and lifetime) is strictly dependent on the presence of BoPz; (*b*) EGFP has poor tendency to self-associate, in contrast with other GFP variants (55); and (*c*) homo-FRET between two identical and close fluorescent molecules does not lead to any changes in fluorescence intensity or lifetime (56).

The rate constants for the dimerization step and its equilibrium dissociation constant close to 2 nM indicated that association of muscarinic monomers was fast (suggesting the existence of vicinal receptors concentrated within membrane micro-domains) and tight, with a half-life close to 6 min (57). Similar parameters have been reported for the interaction of monomers of purified NTS1 receptors (58).

The Pz-induced formation of muscarinic M1 receptor dimers is a new aspect addressed by this study. It was experimentally addressed through FCS measurements of the molecular brightness, a parameter inherently sensitive to the stoichiometry of a protein complex and capable of distinguishing homo- and hetero-complexes from monomer species in living cells (44, 48, 70). Brightness analysis already provided quantitative information on dimeric and oligomeric species for the epidermal growth factor receptor (71), nuclear receptors (48, 70), and a number of nonreceptor proteins (43).

Using FCS, we show that muscarinic M1 receptors, at the plasma membrane level of HEK cells, predominate as monomers in the absence of ligand and dimerize upon pirenzepine binding. These findings represent an additional example for a GPCR to exist in the basal state as a monomeric species (60, 68, 72, 73).

Although there is no doubt that class C receptors function as stable dimers (59), the ability of class A GPCRs to dimerize and the role of such dimers in signaling is currently a hot topic. Indeed, opinions range from "dimers of rhodopsin-like receptors don't even exist" (60) to "GPCRs always function as dimers" (61). A wealth of information together describing the occurrence of receptor monomers, homo- and heterodimers, and higher order oligomers, of SDS-resistant or noncovalent complexes, of agonist-insensitive, -promoted, or -destabilized dimers are some of the numerous examples that illustrate the complexity and the ambiguity of class A receptor oligomerization (for reviews see Refs. 40, 41, 57).

Evidence for muscarinic receptor oligomerization started with the early days of radioligand binding studies. Complex agonist and antagonist binding properties were interpreted in terms of negative or positive cooperativity and of possible site-site interactions within oligomeric receptor complexes (19, 62–64). Numerous biochemical and immunological approaches, including functional trans-complementation (65), co-immunoprecipitation (66), and reconstitution studies (67), provided additional support to muscarinic oligomerization (39, 40, 68). More recently, the formation of muscarinic receptor homo- and hetero-oligomers was directly addressed using bioluminescence resonance energy transfer (69).

Regarding ligand effects (essentially agonists) on class A GPCRs, contradictory results indicate that upon receptor activation dimers may form, dissociate, or persist (see Ref. 74 for an example). Most studies on muscarinic receptors report on agonist and antagonist insensitivity of their oligomeric status (66, 69), suggesting constitutive and stable receptor oligomers.

Interestingly, the muscarinic MT7 toxin[4] and the antagonist QNB (68) have been shown to stabilize M1 and M2 receptor-receptor interactions, respectively, thus providing independent support to our findings. Moreover, high resolution crystal structures of rhodopsin and β_2-adrenergic receptors (two class A GPCRs), determined in the presence of inverse agonists, pointed to a dimer-like packing (75, 76) possibly stabilized by cholesterol binding to a consensus sequence motif found in many GPCRs, including the five muscarinic acetylcholine receptors (77). Finally, in light of recent studies demonstrating that receptor dimerization is not required for G protein activation and even impedes signaling (58, 78), it is tempting to suggest that antagonists (or inverse agonists) such as pirenzepine might stabilize a dimeric, high affinity desensitized receptor state.

Altogether, this study allows a better understanding of ligand binding mechanisms at muscarinic M1 receptors, within a cellular context. It reports on a combination of FRET and FCS studies that may prove useful in examining the differential impact of agonists and antagonists on the conformational, oligomeric, and/or functional status of GPCRs.

Acknowledgments—We thank Dr. Patrick Keller (MPI-CBG, Dresden, Germany) for the gift of the FP-GPI plasmid, which we termed EGFP-GPI in this study. We thank Drs. J. Garwood and F. Simonin for careful reading of the manuscript. We are grateful to Dr. S. Lecat for critical comments and useful advice. The FCS setup was founded by the Association pour la Recherche Contre le Cancer, the Fondation pour la Recherche Médicale, the Agence Française Contre les Myopathies, the Programme Physique-Chimie du Vivant, and by the RTmfm network from the CNRS.

REFERENCES

1. Hermans, E. (2003) *Pharmacol. Ther.* **99,** 25–44
2. Perez, D. M., and Karnik, S. S. (2005) *Pharmacol. Rev.* **57,** 147–161
3. DeWire, S. M., Ahn, S., Lefkowitz, R. J., and Shenoy, S. K. (2007) *Annu. Rev.*

[4] D. Servent, personal communication.

Physiol. **69,** 483–510
4. Palanche, T., Ilien, B., Zoffmann, S., Reck, M. P., Bucher, B., Edelstein, S. J., and Galzi, J. L. (2001) *J. Biol. Chem.* **276,** 34853–34861
5. Bockaert, J., Fagni, L., Dumuis, A., and Marin, P. (2004) *Pharmacol. Ther.* **103,** 203–221
6. Kenakin, T. (2007) *Trends Pharmacol. Sci.* **28,** 407–415
7. Urban, J. D., Clarke, W. P., von Zastrow, M., Nichols, D. E., Kobilka, B., Weinstein, H., Javitch, J. A., Roth, B. L., Christopoulos, A., Sexton, P. M., Miller, K. J., Spedding, M., and Mailman, R. B. (2007) *J. Pharmacol. Exp. Ther.* **320,** 1–13
8. Deupi, X., and Kobilka, B. (2007) *Adv. Protein Chem.* **74,** 137–166
9. Lohse, M. J., Hoffmann, C., Nikolaev, V. O., Vilardaga, J. P., and Bünemann, M. (2007) *Adv. Protein Chem.* **74,** 167–188
10. Elling, C. E., Frimurer, T. M., Gerlach, L. O., Jorgensen, R., Holst, B., and Schwartz, T. W. (2006) *J. Biol. Chem.* **281,** 17337–17346
11. Li, J. H., Han, S. J., Hamdan, F. F., Kim, S. K., Jacobson, K. A., Bloodworth, L. M., Zhang, X., and Wess, J. (2007) *J. Biol. Chem.* **282,** 26284–26293
12. Liu, P., Ahmed, S., and Wohland, T. (2008) *Trends Endocrinol. Metab.* **19,** 181–190
13. Lecat, S., Bucher, B., Mely, Y., and Galzi, J. L. (2002) *J. Biol. Chem.* **277,** 42034–42048
14. Castro, M., Nikolaev, V. O., Palm, D., Lohse, M. J., and Vilardaga, J. P. (2005) *Proc. Natl. Acad. Sci. U.S.A.* **102,** 16084–16089
15. Caulfield, M. P., and Birdsall, N. J. (1998) *Pharmacol. Rev.* **50,** 279–290
16. Kloog, Y., and Sokolovsky, M. (1978) *Brain Res.* **144,** 31–48
17. Järv, J., Hedlund, B., and Bartfai, T. (1979) *J. Biol. Chem.* **254,** 5595–5598
18. Klein, W. L. (1980) *Biochem. Biophys. Res. Commun.* **93,** 1058–1066
19. Henis, Y. I., and Sokolovsky, M. (1983) *Mol. Pharmacol.* **24,** 357–365
20. Eller, M., and Järv, J. (1988) *Neurochem. Int.* **12,** 285–289
21. Jakubik, J., El-Fakahany, E. E., and Tucek, S. (2000) *J. Biol. Chem.* **275,** 18836–18844
22. Ilien, B., Franchet, C., Bernard, P., Morisset, S., Weill, C. O., Bourguignon, J. J., Hibert, M., and Galzi, J. L. (2003) *J. Neurochem.* **85,** 768–778
23. Tahtaoui, C., Parrot, I., Klotz, P., Guillier, F., Galzi, J. L., Hibert, M., and Ilien, B. (2004) *J. Med. Chem.* **47,** 4300–4315
24. Weill, C., Galzi, J. L., Chasserot-Golaz, S., Goeldner, M., and Ilien, B. (1999) *J. Neurochem.* **73,** 791–801
25. Reich, J. G. (1992) *In Curve Fitting and Modelling for Scientists and Engineers*, McGraw-Hill Inc., New York
26. Bernacchi, S., Stoylov, S., Piémont, E., Ficheux, D., Roques, B. P., Darlix, J. L., and Mély, Y. (2002) *J. Mol. Biol.* **317,** 385–399
27. Avilov, S. V., Piemont, E., Shvadchak, V., de Rocquigny, H., and Mély, Y. (2008) *Nucleic Acids Res.* **36,** 885–896
28. Clamme, J. P., Azoulay, J., and Mély, Y. (2003) *Biophys. J.* **84,** 1960–1968
29. Azoulay, J., Clamme, J. P., Darlix, J. L., Roques, B. P., and Mély, Y. (2003) *J. Mol. Biol.* **326,** 691–700
30. Livesey, A. K., and Brochon, J. C. (1987) *Biophys. J.* **52,** 693–706
31. Kim, S. A., Heinze, K. G., and Schwille, P. (2007) *Nat. Methods* **4,** 963–973
32. Rigler, R., Mets, Ü., Widengren, J., and Kask, P. (1993) *Eur. Biophys. J.* **22,** 169–175
33. Pepperkok, R., Squire, A., Geley, S., and Bastiaens, P. I. (1999) *Curr. Biol.* **9,** 269–272
34. Gautier, I., Tramier, M., Durieux, C., Coppey, J., Pansu, R. B., Nicolas, J. C., Kemnitz, K., and Coppey-Moisan, M. (2001) *Biophys. J.* **80,** 3000–3008
35. Ziessel, R., Ulrich, G., and Harriman, A. (2007) *New J. Chem.* **31,** 496–501
36. Kneen, M., Farinas, J., Li, Y., and Verkman, A. S. (1998) *Biophys. J.* **74,** 1591–1599
37. Heikal, A. A., Hess, S. T., and Webb, W. W. (2001) *Chem. Phys.* **274,** 37–55
38. Heuser, J. E., and Anderson, R. G. (1989) *J. Cell Biol.* **108,** 389–400
39. Angers, S., Salahpour, A., and Bouvier, M. (2002) *Annu. Rev. Pharmacol. Toxicol.* **42,** 409–435
40. Rios, C. D., Jordan, B. A., Gomes, I., and Devi, L. A. (2001) *Pharmacol. Ther.* **92,** 71–87
41. Szidonya, L., Cserzo, M., and Hunyady, L. (2008) *J. Endocrinol.* **196,** 435–453
42. Krichevsky, O., and Bonnet, G. (2002) *Rep. Prog. Phys.* **65,** 251–297
43. Briddon, S. J., and Hill, S. J. (2007) *Trends Pharmacol. Sci.* **28,** 637–645
44. Müller, J. D., Chen, Y., and Gratton, E. (2000) *Biophys. J.* **78,** 474–486
45. Cézanne, L., Lecat, S., Lagane, B., Millot, C., Vollmer, J. Y., Matthes, H., Galzi, J. L., and Lopez, A. (2004) *J. Biol. Chem.* **279,** 45057–45067
46. Philip, F., Sengupta, P., and Scarlata, S. (2007) *J. Biol. Chem.* **282,** 19203–19216
47. Chen, Y., Müller, J. D., Ruan, Q., and Gratton, E. (2002) *Biophys. J.* **82,** 133–144
48. Chen, Y., Wei, L. N., and Müller, J. D. (2003) *Proc. Natl. Acad. Sci. U.S.A.* **100,** 15492–15497
49. Keller, P., Toomre, D., Díaz, E., White, J., and Simons, K. (2001) *Nat. Cell Biol.* **3,** 140–149
50. Sharma, P., Varma, R., Sarasij, R. C., Ira Gousset, K., Krishnamoorthy, G., Rao, M., and Mayor, S. (2004) *Cell* **116,** 577–589
51. Gambin, Y., Lopez-Esparza, R., Reffay, M., Sierecki, E., Gov, N. S., Genest, M., Hodges, R. S., and Urbach, W. (2006) *Proc. Natl. Acad. Sci. U.S.A.* **103,** 2098–2102
52. Luthin, G. R., and Wolfe, B. B. (1984) *Mol. Pharmacol.* **26,** 164–169
53. Hedlund, B., Grynfarb, M., and Bartfai, T. (1982) *Naunyn-Schmiedebergs Arch. Pharmacol.* **320,** 3–13
54. Ghanouni, P., Gryczynski, Z., Steenhuis, J. J., Lee, T. W., Farrens, D. L., Lakowicz, J. R., and Kobilka, B. K. (2001) *J. Biol. Chem.* **276,** 24433–24436
55. Clayton, A. H., Hanley, Q. S., Arndt-Jovin, D. J., Subramaniam, V., and Jovin, T. M. (2002) *Biophys. J.* **83,** 1631–1649
56. Lidke, D. S., Nagy, P., Barisas, B. G., Heintzmann, R., Post, J. N., Lidke, K. A., Clayton, A. H., Arndt-Jovin, D. J., and Jovin, T. M. (2003) *Biochem. Soc. Trans.* **31,** 1020–1027
57. Gurevich, V. V., and Gurevich, E. V. (2008) *Trends Pharmacol. Sci.* **29,** 234–240
58. White, J. F., Grodnitzky, J., Louis, J. M., Trinh, L. B., Shiloach, J., Gutierrez, J., Northup, J. K., and Grisshammer, R. (2007) *Proc. Natl. Acad. Sci. U.S.A.* **104,** 12199–12204
59. Pin, J. P., Kniazeff, J., Liu, J., Binet, V., Goudet, C., Rondard, P., and Prézeau, L. (2005) *FEBS J.* **272,** 2947–2955
60. Chabre, M., and le Maire, M. (2005) *Biochemistry* **44,** 9395–9403
61. Fotiadis, D., Jastrzebska, B., Philippsen, A., Müller, D. J., Palczewski, K., and Engel, A. (2006) *Curr. Opin. Struct. Biol.* **16,** 252–259
62. Potter, L. T., Ballesteros, L. A., Bichajian, L. H., Ferrendelli, C. A., Fisher, A., Hanchett, H. E., and Zhang, R. (1991) *Mol. Pharmacol.* **39,** 211–221
63. Hirschberg, B. T., and Schimerlik, M. I. (1994) *J. Biol. Chem.* **269,** 26127–26135
64. Chidiac, P., Green, M. A., Pawagi, A. B., and Wells, J. W. (1997) *Biochemistry* **36,** 7361–7379
65. Maggio, R., Vogel, Z., and Wess, J. (1993) *Proc. Natl. Acad. Sci. U.S.A.* **90,** 3103–3107
66. Zeng, F. Y., and Wess, J. (1999) *J. Biol. Chem.* **274,** 19487–19497
67. Ma, A. W., Redka, D. S., Pisterzi, L. F., Angers, S., and Wells, J. W. (2007) *Biochemistry* **46,** 7907–7927
68. Park, P. S., and Wells, J. W. (2003) *Biochemistry* **42,** 12960–12971
69. Goin, J. C., and Nathanson, N. M. (2006) *J. Biol. Chem.* **281,** 5416–5425
70. Chen, Y., Wei, L. N., and Müller, J. D. (2005) *Biophys. J.* **88,** 4366–4377
71. Saffarian, S., Li, Y., Elson, E. L., and Pike, L. J. (2007) *Biophys. J.* **93,** 1021–1031
72. Patel, R. C., Kumar, U., Lamb, D. C., Eid, J. S., Rocheville, M., Grant, M., Rani, A., Hazlett, T., Patel, S. C., Gratton, E., and Patel, Y. C. (2002) *Proc. Natl. Acad. Sci. U.S.A.* **99,** 3294–3299
73. Meyer, B. H., Segura, J. M., Martinez, K. L., Hovius, R., George, N., Johnsson, K., and Vogel, H. (2006) *Proc. Natl. Acad. Sci. U.S.A.* **103,** 2138–2143
74. Grant, M., Collier, B., and Kumar, U. (2004) *J. Biol. Chem.* **279,** 36179–36183
75. Palczewski, K. (2006) *Annu. Rev. Biochem.* **75,** 743–767
76. Cherezov, V., Rosenbaum, D. M., Hanson, M. A., Rasmussen, S. G., Thian, F. S., Kobilka, T. S., Choi, H. J., Kuhn, P., Weis, W. I., Kobilka, B. K., and Stevens, R. C. (2007) *Science* **318,** 1258–1265
77. Hanson, M. A., Cherezov, V., Griffith, M. T., Roth, C. B., Jaakola, V. P., Chien, E. Y., Velasquez, J., Kuhn, P., and Stevens, R. C. (2008) *Structure* **16,** 897–905
78. Whorton, M. R., Bokoch, M. P., Rasmussen, S. G., Huang, B., Zare, R. N., Kobilka, B., and Sunahara, R. K. (2007) *Proc. Natl. Acad. Sci. U.S.A.* **104,** 7682–7687